Research article

Maize Sciences, 2026, 1: 100017

Planting Density and Controlled-Release Urea Proportion Mitigate Nitrogen Loss and Increase Grain Yield in Summer Maize

Shihong LIU[1], Xiaoqing WANG[1], Yifeng WEI[1], Hang LI[1], Baoyuan ZHOU[2], Baozhong YIN[1]

([1]*College of Plant Protection, Hebei Agricultural University, Baoding 071001, Hebei, China;* [2]*Institute of Crop Science, Chinese Academy of Agricultural Sciences/State Key Laboratory of Crop Gene Resources and Breeding, Beijing 100081, China*)

Abstract: Coordinating planting density and controlled-release urea (CRU) application can maintain summer maize yield while reducing nitrogen (N) losses, although the optimal CRU proportion at different densities remains unclear. A two-year field experiment was conducted in Xinji, Hebei, China (2024–2025) to evaluate three densities (6.75×10^4, 8.25×10^4, and 9.75×10^4 plants ha^{-1}; D1–D3) and four CRU proportions (0%, 30%, 50%, and 70% of total N; R0–R70) at 210 kg N ha^{-1}. Increasing the CRU proportion delayed and attenuated the NH_3 volatilization peak and lowered the 10-d increase in 40–100 cm NO_3^--N storage by 32.0% (R50) and 42.4% (R70). At maturity, aboveground N accumulation under R50 was 31.0% higher than that under R0, and post-anthesis dry matter under R70 contributed 88.8%–92.4% of grain dry matter. Higher planting density increased ear number but reduced kernels per ear and 100-kernel weight, so yield peaked at D2 rather than D3. D2R50 produced the highest yield in both years, exceeding D2R0 by 11.2%–14.6%. Random forest analysis placed the yield-response optimum near 8.28×10^4 plants ha^{-1} and 51% CRU, close to D2R50. In contrast, the TOPSIS multi-objective evaluation ranked D3R70 first when N-loss indicators were weighted heavily, whereas D2R50 ranked fourth. Thus, D2R50 is the yield-optimal combination, whereas high-density, high-CRU combinations better balance productivity and N-loss mitigation.

Key words: summer maize; planting density; controlled-release urea; nitrogen loss; grain yield

INTRODUCTION

Nitrogen (N) availability strongly influences canopy development, dry-matter production, and grain yield in summer maize. Warm, wet summer conditions in the North China Plain can accelerate N transformation. When conventional urea is applied at sowing, N release early in the season may exceed crop demand, increasing ammonia (NH_3) volatilization and downward nitrate (NO_3^--N) movement while leaving less N available later in the season (Guo et al., 2024; Hou et al., 2024). Synchronizing fertilizer N release with crop demand is therefore important for maintaining yield and limiting N losses. However, few studies have evaluated different controlled-release urea (CRU) proportions at a fixed total N rate across contrasting planting densities. How density and CRU proportion jointly influence the progression from early-season N loss to late-season yield formation also remains unclear.

Planting density influences the balance between plant population size and individual-plant productivity. Moderate increases in density generally raise ear number per unit area, whereas excessive density intensifies competition for light, water, and nutrients, there by reducing kernels per ear and kernel weight (Zhang et al., 2022; Liu et al., 2022). A recent meta-analysis showed that yield responses to planting density differ among maize-growing regions (Zhang et al., 2025). Nitrogen management can influence this response because denser stands require adequate N to sustain assimilate production and grain filling during reproductive growth (Liu et al., 2022; Tian et al., 2024). The agronomic optimum therefore depends on both planting density and the timing of N availability.

CRU can prolong N availability by slowing its release. Studies have reported reduced NH_3 volatilization, changes in soil NO_3^--N distribution, improved crop N uptake, and maintained or increased

Received: 13 October 2026; **Accepted:** 5 November 2026
Corresponding author: Baozhong Yin (yinbaozhong@hebau.edu.cn)
©The Author(s) 2026. Published by Higher Education Press
This is an open access article under the CC BY license (http://creativecommons.org/licenses/by/4.0)
https://doi.org/10.2738/MS.2026.0017

maize yield when CRU is applied alone or blended with conventional urea (Sun et al., 2023; Guo et al., 2024; Li et al., 2024). These effects vary with the proportion of total N supplied as CRU. A low CRU proportion may provide insufficient N during reproductive growth, whereas a proportion that exceeds crop requirements may offer little additional yield benefit (Zheng et al., 2016; Guo et al., 2017).

We hypothesized that increasing the CRU proportion would reduce NH_3 volatilization and deep-soil NO_3^--N accumulation while sustaining reproductive-stage N supply, with yield gains diminishing beyond an intermediate proportion, and that planting density would modulate this response. A two-year field experiment combining three planting densities with four CRU proportions was therefore conducted to (1) quantify NH_3 volatilization and downward NO_3^--N redistribution, (2) determine effects on N accumulation, dry-matter production, grain filling, and (3) identify a density–CRU combination that best balances yield with N-loss mitigation.

RESULTS

Effects of planting density and CRU proportion on NH_3 volatilization and soil NO_3^--N redistribution

NH_3 volatilization

NH_3 volatilization flux exhibited a single peak in each year, occurring 2–5 d after fertilization (Fig. 1). Peak flux occurred at 2–3 d under R0, 3–4 d under R50, and 4–5 d under R70, with R30 showing an intermediate timing (2–4 d). Neither peak timing nor magnitude differed significantly among planting densities at a given CRU proportion. Mean 35-d cumulative NH_3 volatilization across treatments was higher in 2025 (22.5 kg N ha^{-1}, range 17.8–27.7 kg N ha^{-1}) than in 2024 (20.4 kg N ha^{-1}, range 16.0–24.9 kg N ha^{-1}), although the patterns of treatment response were similar in both years.

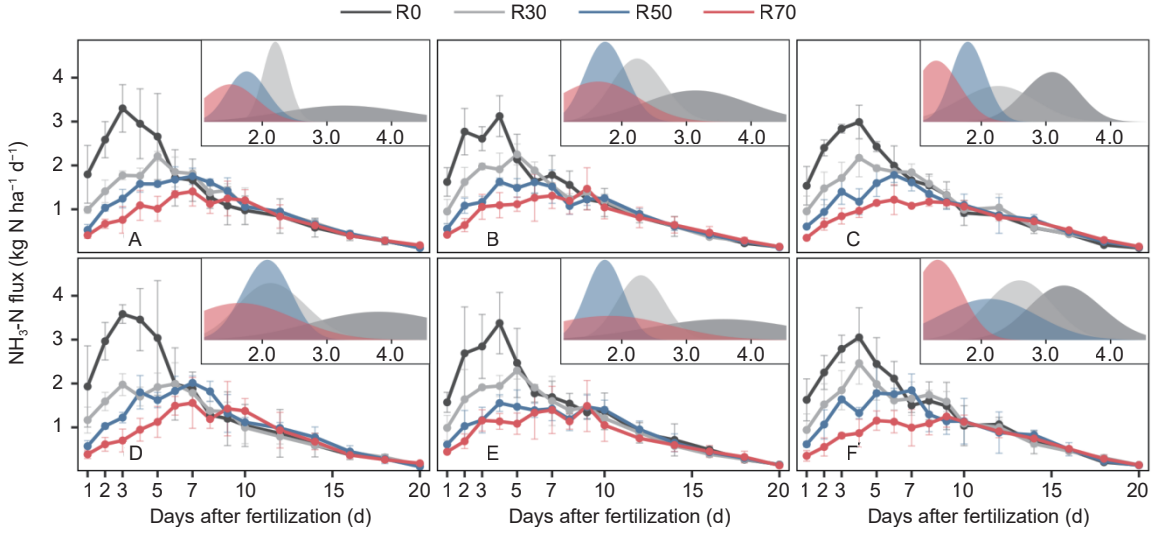


Fig. 1. NH_3 volatilization under different planting densities and CRU proportions.
Note: Panels (A–C) show D1–D3 in 2024, and panels (D–F) show D1–D3 in 2025. Lines and error bars represent mean NH_3-N flux and SD (n = 3), respectively. Insets show kernel-density estimates of peak NH_3-N flux for each CRU proportion. R0, R30, R50, and R70 denote 0%, 30%, 50%, and 70% of total N supplied as CRU, respectively.

Cumulative NH_3 volatilization declined with increasing CRU proportion (Fig. 1). Relative to R0 at the same planting density, R50 and R70 reduced 35-d cumulative NH_3 volatilization by 19.4%–25.2% and 31.7%–34.5%, respectively ($P < 0.05$), whereas the reduction under R30 (11.0%–13.2%) was not statistically significant. The difference between R50 and R70 was not significant, nor was there a significant density effect at a given CRU proportion.

Soil NO_3^--N redistribution

Irrigation promoted downward redistribution of soil NO_3^--N in both years (Fig. 2). Across treatments, NO_3^--N concentrations in the 0–20 cm layer peaked 5 d after irrigation, while those in the 40–100 cm profile increased over the same period. R0 generally showed the highest surface concentration and the greatest accumulation in deeper layers. Higher CRU proportions reduced both the surface concentration

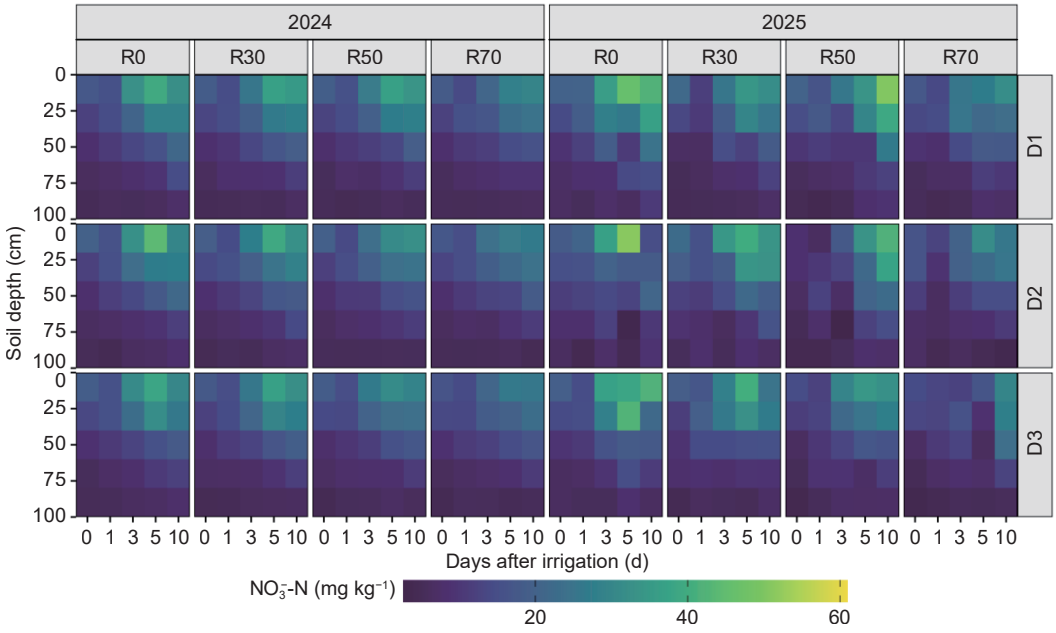


Fig. 2. Temporal and vertical distribution of soil NO_3^--N following irrigation under different planting densities and CRU proportions.
Note: Rows correspond to planting densities D1, D2, and D3; columns are grouped by year (2024 and 2025) and CRU proportion (R0, R30, R50, and R70). The horizontal axis indicates days after irrigation (d), and the vertical axis indicates soil depth (cm). Color represents soil NO_3^--N concentration (mg kg^{-1}).

peak and subsequent accumulation at depth.

The 10-d increase in NO_3^--N storage in the 40–100 cm layer declined as the CRU proportion increased (Table S1). Relative to R0 at the same planting density, R50 and R70 reduced the 10-d increase in 40–100 cm NO_3^--N storage by 30.2%–33.7% and 38.7%–46.1%, respectively, whereas the reduction under R30 was not significant. R50 and R70 did not differ significantly, and planting density had no significant effect at a given CRU proportion.

Effects of planting density and CRU proportion on maize N accumulation and dry-matter production

Aboveground N and dry-matter accumulation

Aboveground N and dry-matter accumulation increased with crop development in both years (Fig. 3). Differences among treatments were limited from three-leaf stage (V3) to twelve-leaf stage (V12) but became more pronounced after the silking stage (R1). From R1 onward, N and dry-matter accumulation were greater under R50 and R70 than

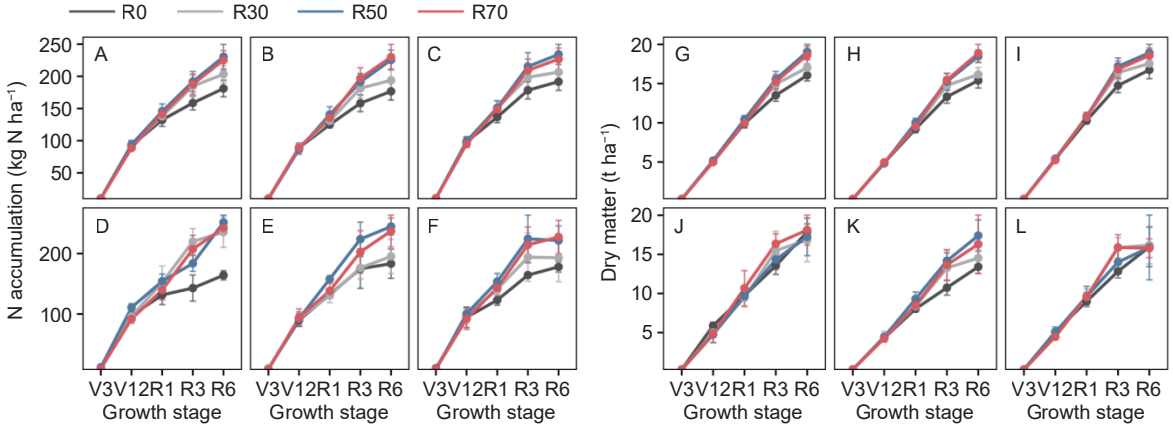


Fig. 3. Aboveground N and dry-matter accumulation under different planting densities and CRU proportions.
Note: Panels (A–F) show aboveground N accumulation, and panels (g)–(l) show aboveground dry-matter accumulation. Panels (A–C) and (G–I) correspond to D1–D3 in 2024; panels (D–F) and (J–L) correspond to D1–D3 in 2025. Values are means ± SD (n = 3). V3, V12, R1, R3, and R6 denote the three-leaf, twelve-leaf, silking, milk, and physiological maturity stages, respectively.

under R0, with the largest differences during milk and physiological maturity stages (R3–R6); the response under R30 was smaller.

At R6, aboveground N accumulation under R50 exceeded that under R0 by 31% (mean across densities and years), whereas the increase under R70 was 24% in 2024 and 34% in 2025; R30 increased accumulation by 9.7%–17.9%. Aboveground N accumulation was the highest under D2R70 in 2024, exceeding D2R0 by 30.3%, whereas D2R50 produced the highest accumulation in 2025, exceeding D2R0 by 33.3%. Post-R1 dry-matter accumulation followed a similar pattern: D1 was lower than D2 and D3 at R6, whereas D2 and D3 generally did not differ significantly. Increasing the CRU proportion from R50 to R70 did not consistently increase either N or dry-matter accumulation.

Dry-matter translocation and post-anthesis accumulation

Higher CRU proportions primarily increased post-anthesis dry-matter accumulation (Table 1). Relative to R0, post-anthesis accumulation increased by 36% under R50 (mean across densities and years) and by 50% in 2024 and 62% in 2025 under R70 ($P < 0.05$). Under R70, post-anthesis accumulation contributed 88.8%–92.4% of grain dry matter, while the contribution of pre-anthesis translocation declined to 11.7%–13.2%. Pre-anthesis dry-matter translocation responded less strongly to CRU proportion than post-anthesis accumulation and declined mainly under R70 (by 0.3–1.1 t ha^{-1} relative to R0). Under R0 and R70, D2 and D3 generally had greater post-anthesis dry-matter accumulation than D1, but planting density did not significantly affect the proportional contribution of post-anthesis accumulation.

Effects of planting density and CRU proportion on maize grain filling and yield

Grain-filling dynamics and logistic-model parameters

Grain-filling rates followed a unimodal pattern across treatments and peaked 30 d after silking (Fig. 4-A to-C, -E to -G). Rates during the early phase (10–20 d after silking) were similar across treatments, whereas R50 and R70 maintained higher rates than R0 during the middle and late phases. D2R50 had the highest peak rate among the 12 treatments in both years. Parameters of the logistic model reflected these differences (Table 2). Relative to R0, the theoretical maximum individual-kernel dry weight (*A*) increased by 7.8%–10.2% under R50 and by 7.3%–12.2% under

Table 1. Dry-matter translocation, post-anthesis accumulation, and their contributions to grain dry matter under different planting densities and CRU proportions.

Treatment	2024				2025			
	DMT (t ha^{-1})	DMA (t ha^{-1})	CR_{DMT} (%)	CR_{DMA} (%)	DMT (t ha^{-1})	DMA (t ha^{-1})	CR_{DMT} (%)	CR_{DMA} (%)
D1R0	2.33 Aa	6.24 Ac	27.2 Aa	72.76 Ac	2.17 Aa	6.60 Ab	29.6 Aa	75.86 Ab
D1R30	1.95 Aab	6.91 Ac	21.9 Ab	77.93 Abc	1.98 Aab	7.14 Ab	25.3 Aa	80.59 Aab
D1R50	1.82 Bb	8.54 Ab	17.5 Ac	82.49 Aab	1.81 Bab	8.13 Ab	18.4 Ab	89.78 Aa
D1R70	1.25 Bc	9.78 Aa	11.7 Bd	91.37 Aa	1.47 Ab	10.87 Aa	12.1 Ac	92.43 Aa
D2R0	2.31 Aab	7.21 Ab	24.3 Aa	75.73 Ab	2.16 Abc	6.61 Ab	25.4 Aa	77.08 Aa
D2R30	2.60 Aa	7.48 Ab	25.7 Aa	74.27 Ab	2.70 Aab	7.78 Ab	27.2 Aa	77.09 Aa
D2R50	2.86 Aa	9.20 Aa	23.8 Aa	76.18 Ab	3.33 Aa	10.26 Aa	24.5 Aa	79.56 Aa
D2R70	1.55 Ab	10.47 Aa	13.2 Ab	88.78 Aa	1.37 Ac	11.55 Aa	12.6 Ab	90.63 Aa
D3R0	2.17 Aab	7.05 Ac	23.6 Aa	76.35 Aab	2.31 Aab	6.90 Ab	25.8 Aa	83.75 Aa
D3R30	2.83 Aa	7.76 Abc	27.0 Aa	73.01 Ab	3.32 Aa	8.00 Aab	29.4 Aa	75.86 Aa
D3R50	2.50 ABa	9.12 Aab	21.5 Aab	78.41 Aab	2.57 ABab	9.83 Aa	21.9 Aab	83.17 Aa
D3R70	1.45 Ab	10.43 Aa	12.5 ABb	89.79 Aa	1.41 Ab	10.07 Aa	11.9 Ab	89.54 Aa

Note: DMT, pre-anthesis dry-matter translocation; DMA, post-anthesis dry-matter accumulation; CR_{DMT} and CR_{DMA}, the respective contributions of DMT and DMA to grain dry matter (%). Different uppercase letters indicate significant differences among planting densities at the same CRU proportion; different lowercase letters indicate significant differences among CRU proportions at the same planting density ($P < 0.05$).

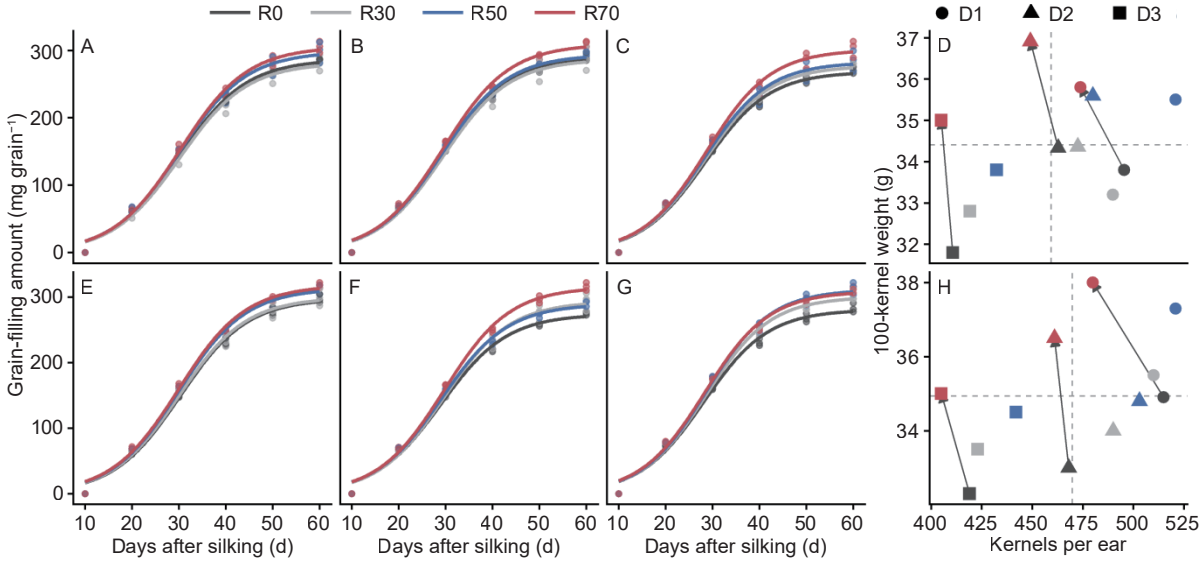


Fig. 4. Grain-filling dynamics and the relationship between kernels per ear and 100-kernel weight across treatments.
Note: Panels (A–C) and (E–G) correspond to planting densities D1–D3 in 2024 and 2025, respectively. Points represent observed means (n = 3), and solid lines represent fitted logistic curves. Panels D and H show the relationship between kernels per ear and 100-kernel weight; colors indicate CRU proportion, and symbols indicate planting density. Arrows show the change from R0 to R70 within each density, and dashed lines indicate overall means.

Table 2. Grain-filling parameters under different planting densities and CRU proportions.

Treatment	2024				2025			
	A (mg grain^{-1})	V_{max} (mg grain^{-1} d^{-1})	T_{max} (d)	T (d)	A (mg grain^{-1})	V_{max} (mg grain^{-1} d^{-1})	T_{max} (d)	T (d)
D1R0	344.76 Aa	9.31 Aa	27.59 Aa	72.31 Ab	352.85 Ab	9.33 Ab	26.31 Aa	73.06 Aa
D1R30	338.64 Aa	9.14 Aa	27.66 Aa	72.59 Aab	372.92 Aa	10.19 Aa	26.86 Aa	73.76 Aa
D1R50	362.10 Aa	9.78 Aa	27.32 Aa	73.82 Aab	388.77 Aa	10.67 Aa	27.11 Aa	74.17 Aa
D1R70	365.16 Aa	9.86 Aa	27.85 Aa	74.50 Aa	383.30 Aa	10.07 Aa	26.67 Aa	74.61 Aa
D2R0	350.19 Ac	9.46 Ac	27.66 Aa	69.45 Ba	367.45 Aa	10.10 Aa	27.17 Aa	70.59 Ba
D2R30	350.49 Ac	9.46 Ac	27.35 Aa	70.79 Aa	375.39 Aa	9.92 Aa	26.93 Aa	71.39 Ba
D2R50	363.05 Ab	9.80 Ab	26.95 Aa	71.42 Ba	355.98 Ab	9.61 Ab	27.83 Aa	73.06 Aa
D2R70	376.50 Aa	10.17 Aa	27.46 Aa	71.44 Ba	362.10 Ab	9.78 Ab	27.42 Aa	73.76 Aa
D3R0	324.36 Bc	8.76 Bc	27.37 Aa	67.78 Cb	380.46 Aa	10.27 Aa	27.29 ABa	74.17 Aa
D3R30	334.56 Abc	9.03 Abc	27.42 Aa	68.82 Aab	387.60 Aa	10.47 Aa	27.15 Aa	74.61 Aa
D3R50	344.76 Bab	9.31 Bab	27.07 Aa	69.22 Cab	336.60 Bc	9.09 Bc	26.48 Bb	70.59 Ba
D3R70	357.00 Aa	9.64 Aa	28.01 Aa	70.12 Ba	346.80 Abc	9.36 Abc	27.75 Aa	71.39 ABa

Note: A, theoretical maximum individual-kernel dry weight; V_{max}, maximum grain-filling rate; T_{max}, time to maximum grain-filling rate; T, effective grain-filling duration. Different uppercase letters indicate significant differences among planting densities at the same CRU proportion; different lowercase letters indicate significant differences among CRU proportions at the same planting density ($P < 0.05$).

R70, with the largest gains at D2 in both years; R50 and R70 did not differ. The time to maximum grain-filling rate (T_{max}) varied only from 26.3 to 28.0 d across treatments. The effective duration of grain filling (T) decreased with increasing density, whereas R50 and R70 extended T by 1.3–2.5 d relative to R0.

The relationship between kernels per ear and 100-kernel weight (Fig. 4-D and -H) helps explain why R50 produced the highest yield. At each density, increasing the CRU proportion shifted treatment points from the lower-right (more kernels, lower kernel weight) toward the upper-left (fewer kernels,

higher kernel weight). R50 occupied the upper-right region and had 7.5%–9.1% more kernels per ear than R70, with only a 1.5%–4.7% reduction in 100-kernel weight.

Grain yield and yield components

Increasing planting density raised ear number but reduced kernels per ear and 100-kernel weight; grain yield therefore peaked at D2 rather than D3 (Fig. 5). Averaged across CRU proportions, D2 outyielded D1 by 12.6%–13.7% and D3 by 1.4%–2.1%. At a given density, CRU proportion changed ear number by no more than 5% but affected kernels per ear and 100-kernel weight by up to 12%; these two components therefore accounted for the yield response. R50 produced the highest grain yield across all six density–year combinations. The yield advantage of R50 over R0 increased with planting density: the gain was 8.1%–9.6% under D1 and 12.2%–14.7% under D2 and D3. In both years, D2R50 produced the highest yield, exceeding D2R0 by 11.2% in 2024 and 14.6% in 2025.

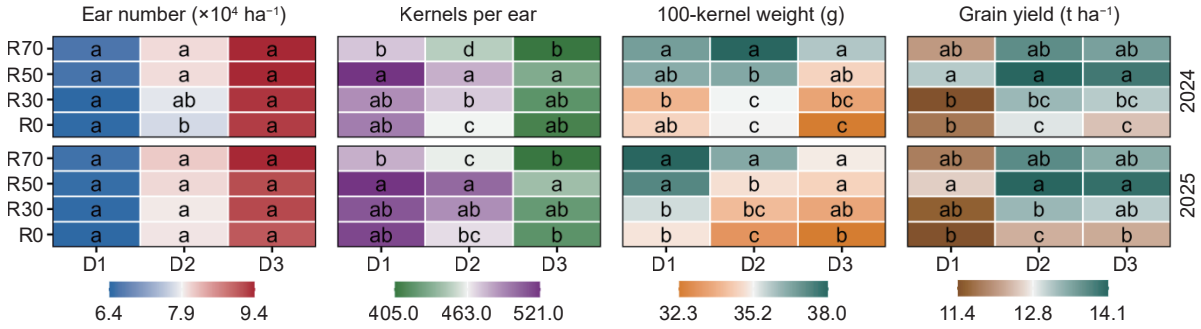


Fig. 5. Grain yield and yield components under different planting densities and CRU proportions.

Note: Values are treatment means. Different lowercase letters indicate significant differences among CRU proportions within the same planting density and year ($P < 0.05$). Colors are scaled independently for each yield variable.

Across years and planting densities, R50 yielded 2.7%–5.4% more than R70, reflecting a trade-off between kernels per ear and 100-kernel weight. R50 maintained 7.5%–9.1% more kernels per ear than R70 despite a 1.5%–4.7% reduction in 100-kernel weight. Under R70, the higher controlled-release fraction may have limited early-season N availability during ear differentiation, lowering kernels per ear relative to R50. The reduction in kernel number outweighed the modest gain in 100-kernel weight associated with delayed senescence.

Integrated analysis of density–CRU responses

Path analysis and multi-objective evaluation

The TOPSIS (technique for order of preference by similarity to ideal solution) evaluation highlighted a trade-off between grain yield and N-loss indicators (Fig. 6-A). D3R70 ranked first in both years (scores of 0.902 and 0.958), whereas D2R50, the highest-yielding treatment, ranked fourth, with D2R70 and D1R70 in between. N-loss indicators therefore had a stronger influence on the TOPSIS ranking than grain yield. Raising the weight assigned to grain yield to 0.7 or higher moved D2R70 ahead of D3R70 (Fig. 6-C), suggesting that D3R70 ranked highest primarily because of its greater N-loss mitigation, whereas D2R70 offered a more favorable balance between productivity and environmental cost.

The structural equation model (SEM) linked this trade-off to different pathways associated with CRU proportion and planting density (Fig. 6-D). CRU strongly reduced N loss (standardized path coefficient = −0.94, $P < 0.001$), while planting density showed no significant direct effect on N loss. Both CRU proportion and planting density tended to increase N supply (0.64 and 0.21, respectively, $P < 0.1$), while the path from N loss to N supply was not significant (−0.21). For grain filling, CRU had a positive effect (0.52, $P < 0.05$) and planting density had a negative effect; N supply had no significant direct effect on grain filling. Grain yield increased significantly with N supply and marginally with grain filling, whereas the direct path from CRU to yield was marginally negative and that from planting density to yield was positive. The marginally negative direct CRU–yield path does not necessarily indicate a yield penalty. Instead, the benefits of CRU were associated with lower N loss and improved late-season N supply, leaving little independent direct effect after accounting for N supply. The model accounted for

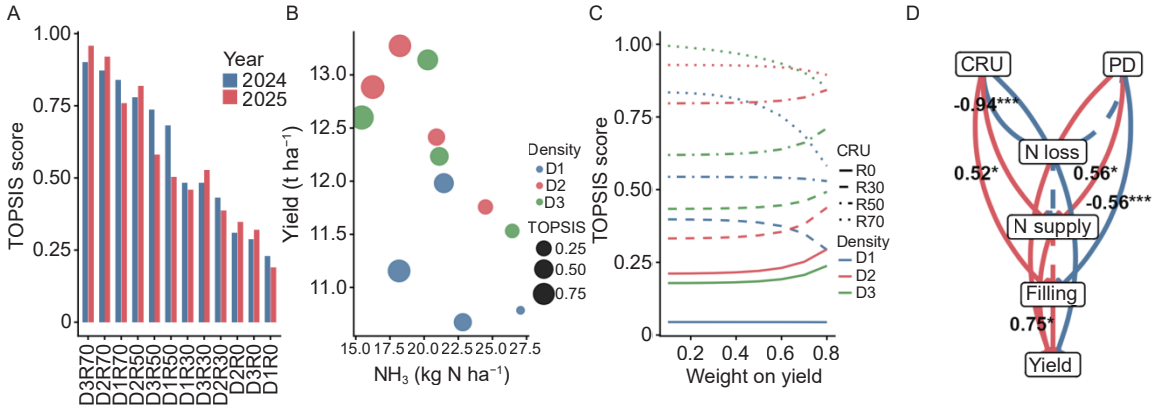


Fig. 6. Multi-objective evaluation and pathway analysis under different planting densities and CRU proportions.
Note: **A**. TOPSIS scores for the 12 treatments in 2024 and 2025, ordered by their 2024 scores. **B**. Relationship between 35-d cumulative NH_3 volatilization and grain yield; point color represents planting density, and bubble size represents the TOPSIS score. **C**. Sensitivity of TOPSIS scores to grain-yield weight; the dashed line indicates equal weighting. **D**. Piecewise structural equation model with standardized path coefficients (n = 24 treatment–year combinations).Solid arrows denote paths with $P < 0.1$; paths with $P < 0.05$ are further marked with asterisks (***$P < 0.001$; *$P < 0.05$), whereas marginally significant paths ($0.05 \le P < 0.1$) carry no asterisk. Dashed arrows denote non-significant paths ($P \ge 0.1$). Red and blue arrows indicate positive and negative effects, respectively.

93%, 84%, 95%, and 84% of the variation in N loss, N supply, grain filling, and yield, respectively.

Yield thresholds for planting density and controlled-release urea proportion

Random-forest partial-dependence analysis predicted the highest yield at 8.28 × 10^4 plants ha^{-1} (Fig. 7-A), with lower predicted yields at either side of this density. The yield response to CRU proportion reached a plateau near 50% (Fig. 7-B), consistent with the absence of a further yield increase from R50 to R70. Among the three predictors, year had the highest permutation importance (35.1% IncMSE), followed by planting density (22.5%) and CRU proportion (10.9%) (Fig. 7-C); the high importance of year reflects the marked differences between 2024 and 2025. The two-dimensional partial-dependence surface indicated a maximum near 8.28 × 10^4 plants ha^{-1} and 51% CRU (Fig. 7-D), close to the D2R50 treatment combination.

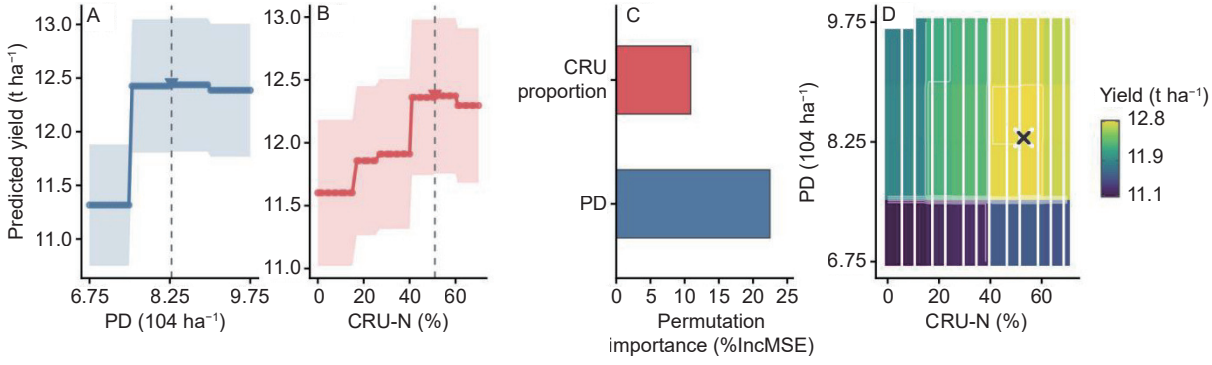


Fig. 7. Random-forest analysis of grain-yield responses to planting density and CRU proportion.
Note: **A**. Partial dependence of grain yield on planting density (PD). **B**. Partial dependence of predicted grain yield on CRU proportion; the dashed line indicates the response maximum. **C**. Permutation importance (% IncMSE) of the displayed predictors; year was also included in the model to account for inter-annual variation. **D**. Two-dimensional partial-dependence surface for PD and CRU proportion; the white cross indicates the predicted maximum.

DISCUSSION

Effects of planting density and CRU proportion on N losses

Increasing the CRU proportion lowered and delayed NH_3 volatilization peaks and reduced NO_3^--N accumulation in the 40–100 cm layer. These findings are consistent with reports that partially replacing conventional urea with CRU can reduce gaseous N loss and nitrate leaching (Zheng et al., 2016; Hou et al., 2024; Guo et al., 2024; Qiao et al., 2025). The reduction in NH_3 volatilization observed here was

smaller than the mean reduction of 54.1% reported in a global meta-analysis of 822 observations in maize, in which resin-based coatings achieved the largest reduction (Qiao et al., 2025). This difference may reflect the use of water-based polymer-coated CRU rather than resin-coated CRU, together with the 50% and 30% conventional urea fractions in R50 and R70. The reduction in deep-soil NO_3^--N accumulation is comparable to the value reported for a 70% CRU blend in Northeast China (Hou et al., 2024). The somewhat larger reduction observed in this study may be associated with higher irrigation inputs at the study site, which increase leaching potential and thus the scope for CRU to limit downward N movement. Nitrate accumulation in deeper soil layers and subsequent leaching are well-documented N-loss pathways in intensive wheat–maize systems of the North China Plain (Ju et al., 2009).

The lower, delayed NH_3 peaks under R50 and R70 may result from the polymer coating, which slows urea dissolution and reduces the substrate available for urease-catalyzed hydrolysis shortly after fertilization (Shaviv, 2001). The smaller increase in deep-soil NO_3^--N storage under CRU blends is consistent with delayed N release from coated granules, which may limit the mineral N available for downward movement during irrigation (Shaviv, 2001; Hou et al., 2024). These processes primarily affect the early-season N pool and showed little dependence on planting density.

The limited response of NH_3 volatilization and deep-soil NO_3^--N accumulation to planting density suggests that early-season N dynamics depended more on fertilizer release and irrigation than on crop demand. By contrast, planting density strongly influenced yield components and grain filling later in the season. Thus, planting density and CRU proportion influence different aspects of N dynamics: CRU affects the timing and magnitude of early N losses, whereas density mainly affects crop N acquisition and use during reproductive growth (Tian et al., 2024).

Effects of planting density and CRU proportion on N accumulation and dry-matter production

Differences in N and dry-matter accumulation became most apparent after R1, when R50 and R70 exceeded R0. This pattern is consistent with the delayed N release and extended nutrient availability expected from CRU (Zheng et al., 2016). Greater post-anthesis dry-matter accumulation under R50 and R70 suggests that sustained N availability supported assimilate production during reproductive growth, reducing reliance on remobilized pre-anthesis reserves. Similar responses have been reported for CRU–urea blends in maize: a 2:1 CRU-to-urea mixture increased grain yield by 18.3%–22.8% by enhancing post-anthesis carbon–nitrogen coordination (Li et al., 2026), and appropriate CRU–urea mixtures improved post-silking growth and grain filling by optimizing root development and delaying leaf senescence (Zheng et al., 2023; Li et al., 2024). The contribution of post-anthesis accumulation under R70 is consistent with values reported for high-yielding maize under optimized N management (Guo et al., 2017; Wu et al., 2024).

The lower contribution of pre-anthesis translocation (11.7%–13.2%) suggests reduced reliance on remobilized reserves, a pattern often associated with a longer effective grain-filling period and greater yield potential (Wei et al., 2019; Zheng et al., 2023). Most of the benefit of CRU for post-anthesis N and dry-matter accumulation was achieved at 50% CRU, with no consistent additional increase under R70. Once N supply meets crop demand, a further increase in the CRU proportion may not enhance assimilate production, although it may still reduce N losses (Zhang et al., 2024).

Effects of planting density and CRU proportion on yield and threshold responses

The yield response to planting density reflected a source–sink trade-off. Increasing density raised ear number, but reductions in kernels per ear and 100-kernel weight prevented D3 from surpassing D2 in yield. Similar compensatory responses among yield components have been reported in high-density maize systems (Liu et al., 2022; Zhang et al., 2025). The yield plateau beyond 50% CRU is consistent with studies of CRU blends in wheat–maize systems, where yield first increased and then declined as the CRU proportion rose, with intermediate blends outperforming either urea source alone (Zheng et al., 2016; Guo et al., 2017; Fan et al., 2025). A global meta-analysis of 822 observations similarly found an average yield increase of 6.5% when CRU replaced conventional urea in maize, with polymer-coated urea the most effective coating type for improving nitrogen use efficiency (NUE, 35.4%) (Qiao et al., 2025). The yield advantage of R50 over R0 in this study

(8.1%–14.7%) was within this range.

The yield advantage of R50 increased with planting density. Although this interaction has seldom been quantified in CRU-blending studies, it is consistent with greater demand for sustained N availability in denser canopies during reproductive growth (Zhang et al., 2022; Tian et al., 2024). D2R50 produced the highest yield in both years, exceeding D2R0 by 11.2% in 2024 and 14.6% in 2025, suggesting that the yield-maximizing CRU proportion was consistent across years at this site. However, the model-derived optima (8.28×10^4 plants ha^{-1} and 51% CRU) should be viewed as approximate response regions rather than precise thresholds, given that only three densities and four CRU proportions were evaluated.

Limitations and practical implications

Several limitations of this study should be noted. First, this study was conducted at a single site with a fixed N rate (210 kg N ha^{-1}), with only three planting densities and four CRU proportions tested, which restricted the extrapolation of findings to wider agro-ecological conditions. Second, the results are based on a single cultivar and two growing seasons, and the relative ranking of treatments may shift with soil type, rainfall pattern, and genotype. Third, the N-loss budget is partially incomplete because N_2O emissions and nitrate leaching below 100 cm were not measured. Practically, under yield-oriented management, D2R50 (8.25×10^4 plants ha^{-1} with 50% of total N supplied as CRU) is recommended because it produced the highest yield in both years; where reducing N losses is the main priority, D3R70 provides the greatest mitigation, and D2R70 becomes preferable when grain yield is assigned a weight of 0.7 or more, with a yield sacrifice of only 2.7%–5.4% relative to R50.

MATERIALS AND METHODS

Experimental site

The field experiment was conducted during the summer maize growing seasons of 2024 and 2025 at Xixie Village, Mazhuang Township, Xinji, Hebei Province, China (37.97°N, 115.22°E). The experimental soil was classified as clay loam. Before the experiment, soil bulk density was measured by the core method in 20-cm increments to a depth of 100 cm, with values of 1.50, 1.51, 1.45, 1.42, and 1.44 g cm^{-3} for the 0–20, 20–40, 40–60, 60–80, and 80–100 cm layers, respectively. These values were used to calculate soil nitrate-N storage. Baseline physicochemical properties of the topsoil (0–20 cm) were as follows: organic matter 18.8 g kg^{-1}, total nitrogen 1.28 g kg^{-1}, alkali-hydrolyzable nitrogen 65.8 mg kg^{-1}, available phosphorus 23.8 mg kg^{-1}, and available potassium 130.6 mg kg^{-1}. Maize was sown on 15 June in both years. It was harvested on 7 October in 2024 and on 15 October in 2025, when rainfall delayed harvesting.

Experimental design

The maize cultivar used was ND372 (Nongda 372; national approval number Guoshen Yu 20252003). A two-factor randomized block design combined three planting densities with four controlled-release urea (CRU) proportions, yielding 12 treatment combinations. Planting densities were 6.75, 8.25, and 9.75×10^4 plants ha^{-1}, designated D1, D2, and D3, respectively. The CRU treatments supplied 0%, 30%, 50%, and 70% of the total N input and were designated R0, R30, R50, and R70, respectively. The maize was planted at a uniform row spacing of 60 cm.

All treatments received 210 kg N ha^{-1}. Nitrogen was supplied as conventional urea (46% N) and water-based polymer-coated CRU (46% N; approximately 60-d release period) in the specified proportions. All N was applied as basal fertilizer at sowing. Phosphorus and potassium rates were identical across treatments, with both P_2O_5 and K_2O applied at 90 kg ha^{-1}. Superphosphate and potassium chloride provided P and K, respectively, and were applied once before sowing.

Each treatment was replicated three times, giving 36 plots arranged in randomized blocks. Each plot measured 48 m^2 (10 m × 4.8 m). After sowing and fertilization, each plot received 60 mm of irrigation through a shallow-buried drip irrigation system. An additional 25 mm of irrigation was applied to all plots at the twelve-leaf stage (V12). Thereafter, the crop relied on rainfall for the remainder of the growing season. All field management practices other than planting density and CRU proportion were kept consistent across treatments. The same plots and treatment layout were maintained in 2025 to ensure continuity between years.

Measurement of ammonia volatilization

NH_3 volatilization was measured using the vented-

chamber method (Wang et al., 2004). One PVC sampling chamber was installed in each plot. Each chamber contained two sponge layers soaked in phosphoric acid–glycerol solution: the lower sponge absorbed NH_3 released from the soil, whereas the upper sponge minimized interference from atmospheric NH_3. Sampling began on the day of fertilization and irrigation and continued for 35 d. The lower sponge was replaced every 24 h, and blanks were collected concurrently. After collection, the lower sponges were sealed and transported to the laboratory. They were thoroughly extracted with deionized water, and NH_4^+-N was quantified using a continuous-flow analyzer (AA3, SEAL Analytical, Norderstedt, Germany). NH_3-N volatilization flux for each sampling interval and cumulative volatilization were calculated as follows:

$$F_i = \frac{M_i}{A\,\Delta t_i} \times 0.01$$

$$E = \sum_{i=1}^{n} F_i\,\Delta t_i$$

where F_i is the NH_3-N volatilization flux during the ith sampling interval (kg N ha^{-1} d^{-1}); M_i is the blank-corrected mass of NH_4^+-N absorbed by the lower sponge (mg N); A is the chamber cross-sectional area (0.0177 m^2); Δt_i is the sampling interval (d); and E is cumulative NH_3-N volatilization (kg N ha^{-1}). The factor 0.01 converts mg N m^{-2} d^{-1} to kg N ha^{-1} d^{-1}.

Measurement of soil NO_3^--N

Soil was sampled at 20-cm intervals through the 0–100 cm profile immediately before irrigation at sowing (applied on the sowing date; baseline) and at 1, 3, 5, and 10 d afterward. Cores collected at the same depth within each plot were combined. Fresh soil was passed through a 2-mm sieve, stored at 4 °C, and analyzed promptly. Fresh soil equivalent to 10 g oven-dry soil was extracted with 50 mL of 2 mol L^{-1} KCl at a soil-to-solution ratio of 1:5. After shaking for 60 min, the suspension was filtered, and NO_3^--N concentration in the filtrate was determined using a continuous-flow analyzer (AA3, SEAL Analytical, Norderstedt, Germany) (Zhu et al., 2012). Soil water content was measured at the same time, and NO_3^--N concentrations were reported on an oven-dry soil basis.

NO_3^--N storage in each 20 cm soil layer was calculated as follows. Storage in the 0–40 and 40–100 cm profiles was calculated by summing the relevant layers:

$$S_i = C_i\,BD_i\,H_i \times 0.1$$

where S_i is NO_3^--N storage in the ith soil layer; C_i is the NO_3^--N concentration in that layer on an oven-dry soil basis; BD_i is soil bulk density; and H_i is layer thickness. The change in NO_3^--N storage in the 40–100 cm soil layer from immediately before irrigation to 10 d after irrigation was calculated as:

$$\Delta S_{40-100}(10\text{ d}) = S_{40-100}(10\text{ d}) - S_{40-100}(0\text{ d})$$

where S_{40-100}(10 d) and S_{40-100}(0 d) denote NO_3^--N storage in the 40–100 cm soil layer at 10 d after irrigation and immediately before irrigation, respectively.

Measurement of plant N and dry-matter accumulation

At the three-leaf (V3), twelve-leaf (V12), silking (R1), milk (R3), and physiological maturity (R6) stages, three representative, uniformly growing maize plants were collected from each plot. Plants were divided into leaves, stems with leaf sheaths, and ears. Samples were heated at 105 °C for 30 min and then oven-dried at 75 °C to constant weight. Dry weight was recorded and expressed as dry-matter accumulation per unit area.

Total N concentration in each dried plant organ was measured by the Kjeldahl method (Ministry of Agriculture of the People's Republic of China, 2013). The average of the three plants sampled from each plot was treated as one statistical observation.

Dry-matter translocation and contribution ratios

Dry-matter measurements at R1 and R6 were used to estimate pre-anthesis dry-matter translocation from vegetative organs, post-anthesis aboveground dry-matter accumulation, and their contributions to grain dry matter. At R6, plant material was separated into vegetative organs and grain. The following equations were used:

$$DMT = DM_{R1} - DM_{R6,v}$$

$$DMA = DM_{R6} - DM_{R1}$$

$$CR_{DMT} = \frac{DMT}{DM_g} \times 100$$

$$CR_{DMA} = \frac{DMA}{DM_g} \times 100$$

where DMT is pre-anthesis dry matter translocated from vegetative organs to grain; DMA is post-anthesis aboveground dry-matter accumulation; DM_{R1} is

aboveground dry-matter accumulation at R1; $DM_{R6,v}$ is dry-matter accumulation of vegetative organs at R6; DM_{R6} is total aboveground dry-matter accumulation at R6; DM_g is grain dry-matter accumulation at R6; and CR_{DMT} and CR_{DMA} are the percentage contributions of *DMT* and *DMA* to grain dry matter, respectively.

Measurement of grain-filling characteristics

At silking, plants showing uniform growth, the same silking date, and no visible disease or insect damage were tagged in each plot. At 10, 20, 30, 40, 50, and 60 d after silking, three representative ears were collected from each plot. Kernels were sampled from adjacent rows in the middle of each ear, heated at 105 °C for 30 min, and then oven-dried at 70 °C to constant weight. The mass of 100 dried kernels was measured and used to calculate individual-kernel dry mass.

A logistic equation was fitted to individual-kernel dry mass over time after silking by nonlinear regression, with each plot replicate fitted separately (Wei et al., 2019). The logistic model, grain-filling-rate equation, and derived parameters were defined as follows:

$$W_t = \frac{A}{1 + Be^{-Ct}}$$

$$V_t = \frac{ABCe^{-Ct}}{(1 + Be^{-Ct})^2}$$

$$T_{\max} = \frac{lnB}{C}$$

$$V_{\max} = \frac{AC}{4}$$

where W_t is individual-kernel dry mass at t d after silking; A is the theoretical maximum kernel dry mass; B and C are model parameters; V_t is grain-filling rate at time t; $T_{\max}$ is the time to maximum grain-filling rate; and $V_{\max}$ is the maximum grain-filling rate.

The boundaries between grain-filling phases were determined as follows:

$$t_1 = \frac{lnB - 1.317}{C}$$

$$t_2 = \frac{lnB + 1.317}{C}$$

$$t_3 = \frac{lnB + 4.595}{C}$$

The durations of the gradually increasing, rapid-filling, and slowly increasing phases, together with the effective grain-filling duration, were calculated as follows:

$$T_1 = t_1$$

$$T_2 = t_2 - t_1$$

$$T_3 = t_3 - t_2$$

$$T = t_3$$

where T_1 is the duration of the gradually increasing phase; T_2 is the duration of the rapid-filling phase; T_3 is the duration of the slowly increasing phase; and T is the effective grain-filling duration. Model fit was evaluated using the coefficient of determination (R^2).

Grain yield and yield components

At physiological maturity, ears within a 2 m^2 area of each plot were hand-harvested to determine grain yield. Ten representative ears per plot were air-dried indoors before yield-component measurements. Kernel moisture content was determined using a grain analyzer, and grain yield was adjusted to 14% moisture content.

Data processing and statistical analysis

Statistical analyses were performed in R 4.5.2 (R Core Team, 2025). For each year, the effects of planting density and CRU proportion were assessed by two-way analysis of variance, followed by Duncan's multiple-range test at $P < 0.05$. Logistic equations were fitted to replicate-level plot data using nonlinear regression (nls), and model fit was evaluated using the R^2. TOPSIS was applied to grain yield, 35-d cumulative NH_3 volatilization, and the 10-d increase in 40–100 cm $NO3^-$-N storage; indicators were normalized by vector normalization, with grain yield treated as a benefit indicator and the two N-loss indicators as cost indicators, and a weight-sensitivity analysis was conducted by varying the weight assigned to grain yield. Random forest regression (500 trees) was used to model grain yield as a function of planting density, CRU proportion, and year; partial dependence plots were used to visualize marginal effects, and permutation importance (% increase in mean squared error) was used to rank predictor contributions (Breiman, 2001). A piecewise structural equation model was fitted using the piecewiseSEM package as a set of linear mixed-effects regressions with block as a random effect; model fit was evaluated using Fisher's C test (Lefcheck, 2016), and standardized path coefficients are reported in Fig. 6-D.

CONCLUSION

At a fixed N rate of 210 kg N ha^{-1}, higher CRU proportions reduced NH_3 volatilization and deep-soil NO_3^--N accumulation while improving late-season N and dry-matter accumulation. However, the yield response largely plateaued near 50% CRU. D2R50 produced the highest yield in both years, exceeding D2R0 by 11.2% in 2024 and 14.6% in 2025. Path analysis associated CRU with lower N loss and greater N supply, and indicated a stronger direct effect of N supply on yield than of grain filling. The multi-objective evaluation favored higher CRU proportions when greater weight was assigned to environmental performance. Under the conditions studied, D2R50 is a suitable yield-oriented option, while higher CRU proportions may be preferable when reducing N losses is the main priority.

ACKNOWLEDGEMENTS

This study was funded by the National Key R&D Program of China (Grant No. 2023YFD2301504).

SUPPLEMENTAL DATA

Supplemental data is available at *Maize Sciences* online.

DATA AVAILABILITY

The data that support the findings of this study are available from the corresponding author upon reasonable request.

REFERENCES

Breiman L. 2001. Random forests. *Machine Learning*, **45**: 5−32.

Fan M Y, Chen P, Zhang C, et al. 2025. Effects of combined application of slow-release nitrogen fertilizer and urea on nitrogen uptake, utilization and yield of maize under two tillage methods. *Scientific Reports*, **15**: 5007.

Guo J M, Wang Y H, Blaylock A D, et al. 2017. Mixture of controlled release and normal urea to optimize nitrogen management for high-yielding (>15 Mg ha^{-1}) maize. *Field Crops Research*, **204**: 23−30.

Guo X, Ren H, Ren B Z, et al. 2024. Long-term application of controlled-release urea reduced ammonia volatilization, raising the risk of N_2O emissions and improved summer maize yield. *Field Crops Research*, **306**: 109227.

Hou Y, Xu X, Kong L, et al. 2024. Combining time-variable controlled release urea formulations to improve spring maize yield and reduce nitrogen losses in northeastern China. *European Journal of Agronomy*, **159**: 127268.

Ju X T, Xing G X, Chen X P, et al. 2009. Reducing environmental risk by improving N management in intensive Chinese agricultural systems. *Proceedings of the National Academy of Sciences of the United States of America*, **106**(9): 3041−3046.

Lefcheck J S. 2016. piecewiseSEM: Piecewise structural equation modelling in R for ecology, evolution, and systematics. *Methods in Ecology and Evolution*, **7**: 573−579.

Li H, Zhu Y M, Wang G F, et al. 2024. Maize yield increased by matching canopy light and nitrogen distribution via controlled-release urea/urea adjustment. *Field Crops Research*, **308**: 109284.

Li H, Zhu Y M, Bai M L, et al. 2026. Controlled-release urea optimizes the pathway to yield increase via post-anthesis carbon–nitrogen coordination in maize. *BMC Plant Biology*, **26**: 1265.

Liu G Z, Yang Y S, Guo X X, et al. 2022. Coordinating maize source and sink relationship to achieve yield potential of 22.5 Mg ha^{-1}. *Field Crops Research*, **283**: 108544.

Ministry of Agriculture of the People's Republic of China. 2013. Determination of total nitrogen in plant—Automatic Kjeldahl apparatus method: NY/T 2419–2013. Beijing: China Agriculture Press. (in Chinese)

Qiao Y, Yue G, Mo X, et al. 2025. Controlled-release urea derived from various coating materials on the impacts of maize production: A meta-analysis. *Industrial Crops and Products*, **225**: 120485.

R Core Team. 2025. R: A language and environment for statistical computing. Vienna: R Foundation for Statistical Computing.

Shaviv A. 2001. Advances in controlled-release fertilizers. *Advances in Agronomy*, **71**: 1−49.

Sun D X, Ma X X, Shang Q H, et al. 2023. Applying waterborne polymer coated urea to realize input reduction and one-time basal application of nitrogen fertilizer in summer maize production in Shandong Province. *Journal of Plant Nutrition and Fertilizers*, **29**(5): 912−923.

Tian L B, Shen Z Y, Zhao X T, et al. 2024. Interactive effects of planting density and nitrogen application rate on plant grain yield and water use efficiency of two maize cultivars. *Scientia Agricultura Sinica*, **57**(21): 4221−4237. (in Chinese)

Wang Z H, Liu X J, Ju X T, et al. 2004. Ammonia volatilization loss from surface-broadcast urea: Comparison of vented- and closed-chamber methods and loss in winter wheat-summer maize rotation in North China Plain. *Communications in Soil Science and Plant Analysis*, **35**(19/20): 2917−2939.

Wei S, Wang X, Li G, et al. 2019. Plant density and nitrogen supply affect the grain-filling parameters of maize kernels located in different ear positions. *Frontiers in Plant Science*, **10**: 180.

Wu B, Cui Z, Zechariah E, et al. 2024. Post-anthesis dry matter and nitrogen accumulation, partitioning, and translocation in maize under different nitrate-ammonium ratios in Northwestern China. *Frontiers in Plant Science*, **15**: 1257882.

Zhang H Y, Zhang C R, Sun P, et al. 2022. Optimizing planting density and nitrogen application to enhance profit and nitrogen use of summer maize in Huanghuaihai region of China. *Scientific Reports*, **12**: 2704.

Zhang M, Zhao X R, Han X Q, et al. 2025. Optimizing planting density for enhanced maize yield and resource use efficiency in China: A meta-analysis. *Agronomy for Sustainable Development*, **45**(3): 29.

Zhang Y, Ren W C, Zhu K Y, et al. 2024. Substituting readily available nitrogen fertilizer with controlled-release nitrogen fertilizer improves crop yield and nitrogen uptake while mitigating environmental risks: A global meta-analysis. *Field Crops Research*, **306**: 109221.

Zheng C Y, Li C L, Tian L B, et al. 2023. Mixture of controlled-release and normal urea to improve maize root development, post-silking plant growth, and grain filling. *European Journal of Agronomy*, **151**: 126994.

Zheng W, Zhang M, Liu Z G, et al. 2016. Combining controlled-release urea and normal urea to improve the nitrogen use efficiency and yield under wheat-maize double cropping system. *Field Crops Research*, **197**: 52−62.

Zhu Q, Ma L, Ma Q, et al. 2012. Content of soil mineral nitrogen as influenced by sample extraction and preservation. *Chinese Journal of Eco-Agriculture*, **20**(2): 138−143. (in Chinese)